

Bioinspired Genetic-Algorithm Optimized Ground-Effect Wing Design: Flight Performance Benefits and Aircraft Stability Effects

KARL ZAMMIT, HOWARD SMITH, NOEL SIERRA LOBO, IOANNIS K. GIANNOPOULOS
Centre of Excellence for Aeronautics, School of Aerospace, Transport and Manufacturing,
Cranfield University,
Cranfield, MK43 0AL,
UNITED KINGDOM

Abstract: - This paper presents a bioinspired, genetic-algorithm evolutionary process for Ground-Effect vehicle wing design. The study made use of a rapid aerodynamic model generation and results evaluation computational fluid dynamics vortex lattice method software, supervised by a genetic algorithm optimization Python script. The design space for the aircraft wing parametric features drew inspiration from seabirds, under the assumption of their wings being naturally evolved and partially optimized for proximity flight over water surfaces. A case study was based on the A-90 Orlyonok Russian Ekranoplan, where alternative bioinspired wing variations were proposed. The study objective was to investigate the possible increased flight aircraft performance when using bioinspired wings, as well as verify the static and dynamic aircraft stability compliance for Ground-Effect flight. The methodology presented herein along with the study results, provided an incremental step towards advancing Ground-Effect aircraft conceptual designs using computational fluid dynamics.

Key-Words: - Bioinspiration, Genetic Algorithm, Ground Effect, Ekranoplan, CFD, Vortex Lattice Method

Received: March 1, 2024. Revised: April 19, 2024. Accepted: April 25, 2024. Published: May 2, 2024.

1 Introduction

Wing-in-ground, WIG-craft, are aircraft vehicles that fly near a surface, mostly above water surfaces. The vehicles make use of the Ground Effect (GE) being the increased lift curve slope and reduced induced drag of the main lifting surfaces, [1].

GE effects are broadly understood as wing-span and wing-chord effects, [1]. The wing-span dominant GE is directly related to a reduction in the induced drag, which is proportional to the wing's spanwise length. When a wing is close to the ground, there is insufficient space for the full development of wingtip vortices. Consequently, air pressure leakage from under the wing to the upper section is reduced. Additionally, the ground's effect pushes the vortices outwards, effectively artificially increasing the wing's aspect ratio beyond its geometric value.

The wing-chord dominant GE involves an increase in static pressure of the oncoming air beneath the wing, which could be further enhanced by utilizing wingtip side plates, [2]. The chord-dominant GE enables the wing to generate more lift per unit area, resulting in a higher lift coefficient for the same power input, [1].

The distance between the wing and the ground influences many of the effects experienced during

flight. Three distinct models have emerged from the literature, each focused on a specific height zone above the surface, [3], [4]. The first zone is the operational region between the surface boundary and a flight height corresponding to 20% of the wing-chord length. In this In-Ground-Effect region (IGE), the flow experiences significant constriction in the vertical direction, leading to a predominantly two-dimensional flow with restricted vertical freedom. The second zone is referred to as the region between one wing-chord length and ten wing-span lengths above the ground. Within this zone, the wing's span dominates the model. Inviscid flow models are commonly employed in this region and demonstrate a marginal increase in the Lift to Drag ratio (L/D), compared to the Out-of-Ground-Effect (OGE) flight. A combination of the two models is necessary to accurately capture the aerodynamic behavior of wings operating in the region between 20% - 100% of chord length, [4]. Above ten wing-span lengths, free-flight models used in conventional aerodynamic theory for aircraft design are applicable.

Distinct wing designs can be observed for WIG craft throughout history. Russian Ekranoplans such as the Korabl Market, the A-90 Orlyonok, and the Lun-class craft, used a low aspect ratio straight wing

with minimal taper and twist. In contrast, the German RFB X-114 and Chinese XTW had wings with a significantly low aspect ratio, a very high taper ratio, slightly sweptback leading and trailing edges, and an appreciably large wing setting angle. More recent WIG craft designs include the soon-to-enter service Viceroy Seaglider by Regent, which has a noticeably different wing planform with a high aspect ratio and quasi-organic shape. Taking an evolutionary perspective on the development and design choices in the history of WIG-craft, there has been a gradual transition towards wings resembling sea birds. Based on this observation, the present study aimed to develop WIG-craft wings using nature-inspired seabird wing designs. By leveraging the principles of bioinspiration, the study explored the potential benefits of integrating biologically derived wing planforms whose efficiency is endorsed by the natural evolution process and the possibility of enhancing the design using an optimization algorithmic approach.

2 Bioinspiration

Research has acknowledged that the wing shapes of seabirds may have evolved to optimize flight over the sea surface, [5]. Seabirds predominantly employ soaring rather than flapping flight, while various soaring methods and corresponding wing planforms could be identified from natural observations, [6], [7].

Albatrosses and *Shearwaters* that belong to the order Procellariiforms, have long and narrow wings, well-suited for soaring and gliding through the windy, middle latitudes of the oceans. These birds rely on horizontal movements of the atmosphere to acquire the energy needed for flying, [8]. Their wings are elongated and slender, often of a high aspect ratio, enabling efficient long-distance flight. Their wingtips can be slightly rounded or pointed, and as such, drag is reduced and enhanced maneuverability over water is achieved. Notably, their oceanic flight involves frequent and brief pull-up maneuvers, converting kinetic to potential energy, [8].

Frigatebirds, renowned skilled aerial predators, exhibit remarkable maneuverability and the ability to stay aloft for extended periods, [9]. Their long and narrow wings have a distinct forked or scissor-shaped silhouette. Such a wing planform facilitates dynamic soaring and allows them to exploit marine thermals and ascending air currents to gain altitude, [8]. Their high aspect ratio wings contribute to efficient gliding and soaring, [9].

Pelicans can adapt their wing for fishing purposes, making their structure unique. Characterized by large wings with broad spans and relatively low aspect ratios, they are designed to support frequent takeoffs and landings on water surfaces, [10]. The broad wings provide sufficient lift during low-level flight, and their relatively short length facilitates agile maneuvers, [8], [10]. Pelicans rely on vertical movements, such as diving from the air into water bodies to capture fish.

The research herein chose the A-90 Orlyonok Russian Ekranoplan WIG-craft for an initial benchmark case study. The A-90 main lifting surfaces were subsequently redesigned with three different bioinspired wings from the seabird families mentioned above and evaluated the flying performance which is presented in the following section.

2.1 Bioinspired Wings

The first part of the study herein, aimed at re-designing the wing of the A-90 Orlyonok WIG-craft, effectively substituting it with bioinspired wing designs stemming from the Albatross, the Frigatebird, and the Pelican seabird families. For that purpose, publicly available information such as representative still images and animated videos of the above-mentioned bird families flying above water surfaces were studied. The investigation resulted in the simplified conceptual parametric design proposal shown in Figure 1, where a five-stations, four-wing sections subdivision was proposed, shown superimposed upon a typical seabird wing.

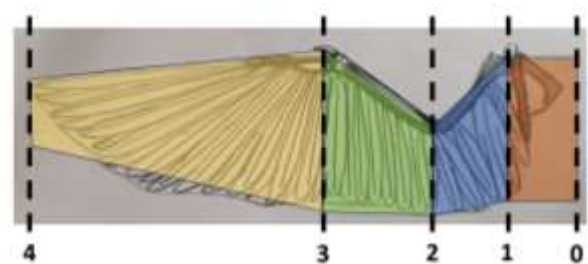


Fig. 1: Sectioned parametric conceptual representation of a seabird wing

The zeroth station shown in Figure 1, represented the birds wing or WIG-craft fuselage centerline, while the first section, between the zeroth and the first station, represented the part of the wing within the main body of the bird or the part of the central wing box embedded within the WIG-craft fuselage. Wing stations one to four were the exposed parts of the wing to the free stream

aerodynamic flow. At each station, the parameters of span, chord, twist, sweep, and anhedral/dihedral angles were set, to closely resemble the seabird soaring above the water surface, as these were captured from the public domain representative imagery material. The wings were designed to be of equal plan area to the A-90 wing. Following the above-stated assumptions, the resulting three bioinspired wing shapes were designed, along with the original A-90 Orlyonok WIG-craft wing. The results are depicted in Figure 2, Figure 3, Figure 4 and Figure 5 and tabulated in Table 1.

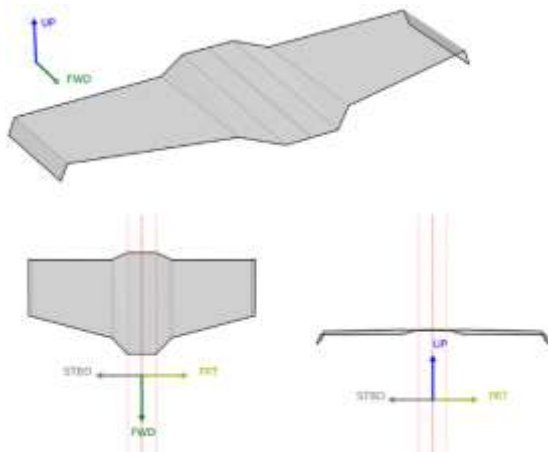


Fig. 2: A-90 Orlyonok wing, [11]

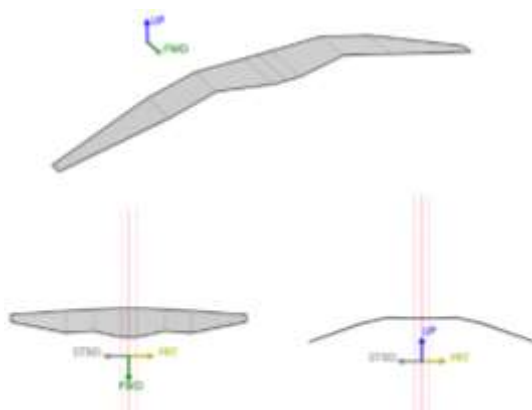


Fig. 3: Albatross bioinspired wing

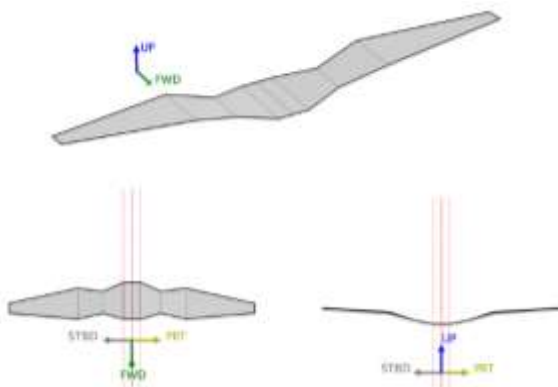


Fig. 4: Frigatebird bioinspired wing

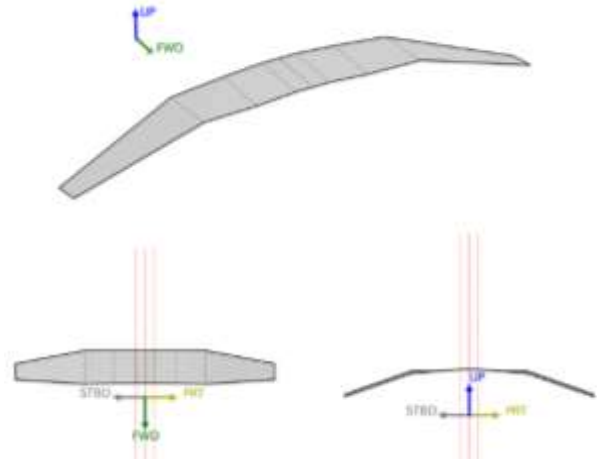


Fig. 5: Pelican bioinspired wing

Table 1. Wing design parameters about Figure 1 wing sections

	Station	Orlyonok	Pelican	Frigatebird	Albatross
Span (m)	0	0.00	0.00	0.00	0.00
	1	2.00	2.00	2.00	2.00
	2	-4.30	6.58	6.80	9.46
	3	15.29	12.78	12.77	16.69
	4	15.78	27.16	29.02	31.11
Chord (m)	0	14.20	6.95	8.60	7.75
	1	14.20	6.95	8.60	7.75
	2	10.90	6.95	5.13	5.80
	3	7.97	7.09	7.24	5.89
	4	7.84	3.34	2.27	1.88
Twist (deg.)	0	0.00	0.00	0.00	0.00
	1	0.00	0.00	0.00	0.00
	2	3.60	0.00	0.00	0.00
	3	3.60	5.00	2.00	0.00
	4	3.60	8.60	-4.00	0.00
Sweep (deg.)	0	0.00	0.00	0.00	0.00
	1	0.00	0.00	0.00	0.00
	2	46.14	0.00	15.74	12.52
	3	14.91	-1.76	-12.69	-3.72
	4	14.91	3.68	-4.86	11.41
Anhedral / Dihedral (deg.)	0	0.00	0.00	0.00	0.00
	1	0.00	0.00	0.00	0.00
	2	2.08	-4.30	11.06	1.97
	3	-1.24	0.00	18.40	-12.61
	4	-83.48	-19.36	3.48	-19.49

2.2 Bioinspired Wings Performance

Having identified three different bioinspired wing planforms potentially suitable for WIG-craft wing design and having established the A-90 as the datum case, an assessment of the bioinspired wing planforms was undertaken to analyze the wing performance and benchmark it against the datum case. The objective was to determine whether the bioinspired wing planforms were viable candidates to use as starting points for an algorithmic evolutionary design process. The methodology followed was similar to the one presented in [12] on the application of a proposed evolutionary algorithm for aerodynamic wing optimization. The computational fluid dynamic software tool of choice

was Athena Vortex Lattice (AVL), [13], a rapid evaluation vortex lattice method computation tool, capable of capturing the GE flying effect. The suitability of AVL for usage in evaluating GE flight has been studied and benchmarked against experimental results, [14]. The four wing sections computationally meshed are shown in Figure 6.



Fig. 6: AVL models of the A-90 and the bioinspired wings

The wing airfoil for the bioinspired wings was assumed to be the same along the wing span and the same as the A-90 wing for all the wings under study.

The objective function that served as metric for evaluating aircraft performance was the Lift to Drag ratio (L/D). The L/D ratio plays an important role in every aspect of aircraft performance such as the range to be traveled for a certain amount of fuel stored, or the takeoff speed required to get airborne that directly affects the size of the engines and the runway length. To assess the bioinspired wing designs performance, the resulting 3D designs' L/D ratio was evaluated using AVL. The computation took place at various heights from the ground, signified by the height from the ground to the wing mean chord non-dimensional parameter (h_{te}/c_m), indicating the distance of the most outboard tip of the trailing edge from the ground (h_{te}), divided by the wing mean chord length (c_m).

The computation for the A-90 Orlyonok wing, set the datum at a maximum L/D ratio of 22.2 at $h_{te}/c_m=0.4$, which approximately corresponded to the operating height of the A-90 at 4.2m, [4]. The L/D ratio was also computed at another three different heights off the ground to diversify the range for comparison. Table 2 presents the corresponding results derived from the AVL simulations, at identical operating parameters and regimes with the datum case being a cruise speed of 104ms^{-1} , [4] and operational height at $h_{te}/c_m=0.4$.

Table 2. Flight performance of the bioinspired wings versus the original A-90 wing

h_{te}/c_m	A-90 wing	Pelican	Frigatebird	Albatross
	L/D (abs)	L/D (% over A-90)		
0.1	26.7	+40.4%	+30.4%	+101.4%
0.4	22.2	+11.1%	+17.5%	+42.5%
0.8	20.3	+9.1%	+18.1%	+36.5%
1.2	19.5	+8.4%	+18.1%	+33.0%

The three bioinspired wings exhibited a superior L/D ratio compared to the A-90 Orlyonok wing with the albatross-inspired wing outperforming the rest. It was interesting to note that while the Pelican-inspired wing had a higher L/D ratio than the Frigatebird derived one closer to the ground at $h_{te}/c_m=0.1$, the latter does better at the higher distance from the ground wing placements. The Pelican-derived wing was the closest to the ground at the wing tips and had an arching shape capable of trapping the incoming air, generating greater lift at lower altitudes, the effect of which lessens with decreasing ground proximity. Conversely, the Frigatebird-inspired wing is lowest at the wing root and has a dihedral-set planform.

The L/D ratio benchmark of the A-90 Orlyonok wing to the three bioinspired versions indicated that the bioinspired wings could offer more efficient alternatives for this type of aircraft. The bioinspired wing design parameters shown in Table 1, assumed the starting point of the genetic algorithm optimization study that followed.

3 Genetic Algorithm Optimization for WIG Wing Design Parameters

Building on the results of the WIG enhanced flight performance in terms of the increased L/D ratio exhibited by the bioinspired wing configurations, further enhancement of the wing designs was sought, through the application of algorithmic optimization. To determine the most suitable algorithm, factors such as the problem's continuous, discrete, or combinatorial nature were considered as well as the dimensionality of the parameter space; the availability of derivative information; the presence of constraints; the characteristics of the objective function such as smoothness, multimodality, and noise. Following some experimentation with different algorithms the Genetic Algorithm (GA) was selected for the current optimization problem. The algorithm drew inspiration from the process of natural selection

operating on a population of potential solutions represented as individuals encoded in a chromosome-like structure, [15], [16], [17]. Implementing the GA in the current research work, involved the representation of the wing parameters as chromosomes, selecting the appropriate genetic operators, and evaluating a fitness function based on wing performance metrics. Multiple iterations of the GA were conducted to properly explore and exploit the solution space. Additionally, implementing mechanisms such as elitism to preserve the best individuals over generations can help maintain high-quality solutions throughout the optimization process. A Python script was developed to conduct the optimization exercise on wing designs evaluated using AVL.

3.1 Chromosome Representation and Population Initialization

The initial step in the GA was to define the genetic makeup of the chromosomes. The wing design geometric variables for the sections shown in Figure 1, were encapsulated within a structured array as genes within each chromosome. Genetic diversity was initiated through the creation of an initial population. This ensemble consisted of the genetic makeup of the abovementioned wing designs; that of the A-90 Orlyonok, Pelican, Frigatebird, and Albatross-inspired wings.

3.2 Fitness Function Definition

The performance metrics selected for qualifying the prevailing wing design parameter sets, were judged according to the following fitness function, eq. (1):

$$Fitness = w_1 \left(\frac{L}{D} \right)_{max,normalised} + w_2 \frac{1}{(C_L - 0.9C_{L,max@70})_{min,normalised}} \quad eq.(1)$$

In the fitness function, a weighted sum of the maximum L/D ratio was taken into account, along with the lift coefficient at 70% of the wing span. The second weighted term is related to the requirement on the shape of the lift curve to meet wing stall characteristics, necessitating at least 10% reserve of lift on the ailerons, when the flow on the root part of the wing is starting to separate, [18]. The weightings w_1 and w_2 were set to 50%. The fitness function shown in eq. (1), was considered to quantify the aerodynamic capability of each chromosome, yielding a fitness score that reflected its optimization potential.

3.3 Chromosomal Crossover

The initial step in the GA was to define the genetic makeup of the chromosomes. Crossover operations facilitate the exchange of genetic material between selected chromosomes. Employing techniques like single-point, multi-point, or uniform crossover, [19], the GA could simulate genetic recombination and introduce diversity and innovation within the population. A single-point crossover mechanism was first explored. Single-point crossover involves selecting a random point along the chromosome and swapping the genetic material between the parents at that point, creating offspring by combining the genetic material from both parents, as shown in Figure 7. However, experience later showed that this method did not introduce enough diversity. The desired crossover mechanism would produce offspring whereby the genetic makeup of both parents would influence every gene. Hence, a blended crossover function was used to combine the genes of the two parents to produce averaged values via a blending parameter that was set to 50%, as shown in Figure 7.

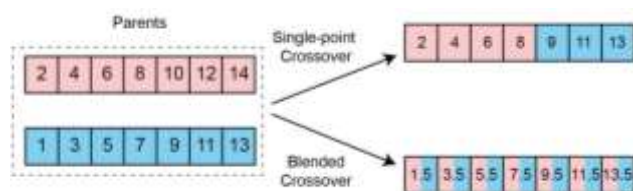


Fig. 7: Single-point crossover and blended crossover

3.4 Genetic Mutation

Mutation can be introduced to diversify the genetic makeup of the GA. Small random changes in chromosomes encourage the exploration of unexplored areas in the design space, enhancing the algorithm's capacity to identify optimal solutions. In the current study, a simple mutation function was initially used; a random perturbation between a range of mutation rates was applied to the entire chromosome. High mutation rates promote exploration by allowing a larger chance for random changes. Very high mutation rates can lead to excessive randomization and slow convergence. Low mutation rates focus more on exploitation by preserving the existing solutions. Very low mutation rates can lead to premature convergence and limit the search space, [19]. While somewhat effective when using a mutation rate in the range of $\pm 10\%$, a need for some adjustments was identified to account for premature convergence or the lack of it. In opting for an adaptive mutation mechanism, a mutation rate of $\pm 25\%$ was dynamically adjusted

during the evolutionary process based on the population's performance or convergence status. Adaptive mutation can help strike a balance between exploration and exploitation, as it allowed for more exploration in the early stages and gradually reduced the mutation rate as the algorithm progressed. When convergence was detected after the first 50% of the generations, the mutation rate was halved. This adjustment prevented seeking convergence prematurely and allowed for finer exploration around the converged region. If convergence did not occur, the mutation rate was doubled to encourage further exploration.

3.5 Selection Mechanism and Population Renewal

A selection mechanism was employed to determine the prevailing chromosomes to proceed to the next generation. Various strategies, such as roulette-wheel selection, tournament selection, or rank-based selection, [20], were considered to favor individuals with higher fitness function evaluation scores, simulating the evolutionary principle of survival of the fittest. Rank-based selection using the principle of elitism was selected in the current study: the fitness values of the parents and offspring were first compared and the individuals with the highest fitness values were carried over as parents for the next generation.

3.6 Termination Criteria

The iterative process of fitness evaluation, selection, crossover, and mutation went through a predetermined number of generations. Each iteration contributed to the refinement of solutions, fostering incremental progress towards optimal designs. At the culmination of the GA process, the optimized geometric variables were extracted from the final generation's chromosomes. These variables represented the refined wing configurations ready for further analysis and evaluation.

3.7 Initial Implementation

Given an initial population of the A-90 Orlyonok wing along the three bioinspired wing versions, and using the abovementioned offspring generation and selection mechanisms, every generation considered a total of ten chromosomes; the four best parent chromosomes carried on from the previous generation and their six offspring. The GA initially was set to iterate through 50 generations for non-dimensional height from the ground $h_{te}/c_m=0.1, 0.4, 0.8, 1.2$. To ensure the robustness and reliability of the results, the process was repeated four times for

each height, meaning that a total of 4,864 wing designs were generated, analyzed, and compared. The process indicated that the algorithm was being heavily influenced by the outcomes of the first few generations. The results differed substantially from each other, often resembling either of the designs in the initial population. Moreover, the examination of the algorithm's performance patterns unveiled a trend toward convergence by the 30th generation. Consequently, the subsequent 20 generations were observed to contribute relatively less substantively to the optimization process, thus prompting reconsideration of the algorithm's implementation.

3.8 Refinement of the Methodology

From the results described above, it was reasoned that the GA was picking up an unwanted bias from the first few generations, primarily attributed to the randomized mutation process. The population renewal mechanism was then altered to include the four wing designs from the initial population in every generation, along with the four chromosomes carried over from the previous generation. As a result, each generation comprised a total of 28 offspring. This adjustment sought to mitigate the algorithm's predisposition to early-stage bias. Mindful of the aforementioned convergence tendency by the 30th generation and the impending project time constraints, a decision was made to limit the GA iterations to 30. However, to maintain the rigor of repeatability and credibility in the results, the algorithm was still run four times for each height-to-chord ratio. This measured approach aimed to strike a balance between achieving meaningful optimization outcomes and respecting the project's practical limitations. A total of 13,504 wing designs were generated, analyzed, and compared as a result of the refined methodology, with the results presented in the following section.

4 Wing Design Results and Discussion

The results of four different optimization cycles numbered (i) to (iv), at the four different non-dimensional height values from the ground are shown in Figure 8 and Figure 9. From these images, the resulting similarity in the designs was evident as well as each optimization cycle had resulted in slightly different wing design parameters, with some features being more consistent and of a smaller statistical deviation than others.

Notably, all wings exhibited an inboard section configured with a dihedral angle, while the remaining two outboard sections featured an

anhedral angle. An increased height-to-chord ratio from $h_{te}/c_m=0.1$ to $h_{te}/c_m=1.2$, led to an increase in the outboard section sweep angle and an overall wing aspect ratio of 135.8% and 6.9% respectively. All wing variations at $h_{te}/c_m=0.1$ had a positive twist angle. Similarly, at $h_{te}/c_m=0.4$, all sections exhibited a positive twist except for the outboard section, where a negative twist resulted. At $h_{te}/c_m=0.8$ and $h_{te}/c_m=1.2$, all sections adopted a negative twist angle.

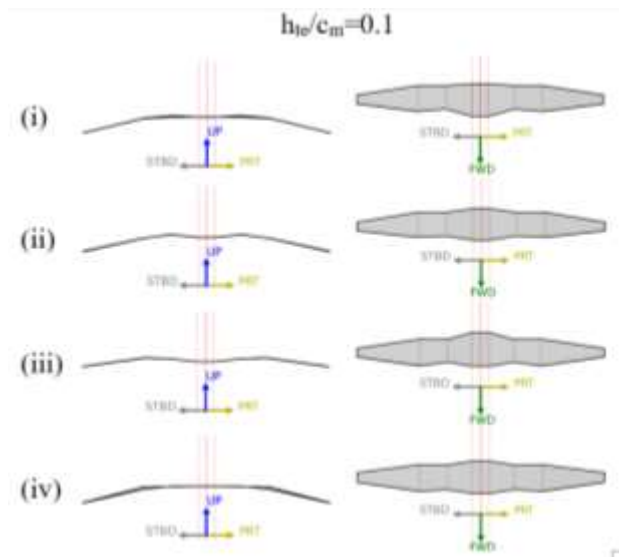


Fig. 8: Wing design results for four different optimization cycles at $h_{te}/c_m=0.1$

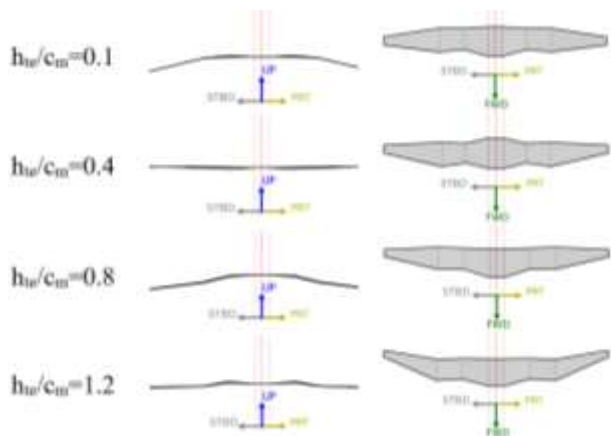


Fig. 9: Wing design results for four different non-dimensional heights h_{te}/c_m

Considering the increase in sweep and aspect ratio at greater heights, suggested an adaptation to higher flight conditions. Higher sweep reduces drag at higher speeds, which became more relevant as the wing moved away from the ground effect. The observed trends could be attributed to a combination of ground effect, aerodynamic interactions, and

design goals. Each height-to-chord ratio likely represents a unique balance of these factors to optimise the L/D ratio and overall performance. The observed changes in the wing profile reflect the algorithm's effort to maintain efficient lift generation while adapting to the reduced ground effect.

Wings at $h_{te}/c_m=0.1, 0.8, 1.2$, had appreciable amounts of anhedral and dihedral, creating a more arched appearance. At $h_{te}/c_m = 0.1$, the wing was closest to the ground experiencing a strong ground effect, which led to air being trapped under the wing, contributing to the observed arched shape. The interaction between the wing and the ground increased the risks of flow separation and stall due to the potential for intricate flow patterns, vortex shedding, and alterations in the effective angle of attack, necessitating the arched wing contour to alleviate these effects. As the height-to-chord ratio increases, the risk of stall may decrease, allowing for a flatter wing design.

The results for $h_{te}/c_m=0.4$, may be seen as outliers to the rest. The wings appeared to be almost flat with minimal anhedral or dihedral. The reduced anhedral and dihedral might signify a compromise between roll stability, discussed later, and minimizing tip vortex effects while being mildly influenced by the ground effect. The relatively neutral appearance implied a design focus on maintaining aerodynamic efficiency over a broad range of operating conditions.

At $h_{te}/c_m=0.8$, and $h_{te}/c_m=1.2$, the resurgence of the anhedral and dihedral akin to $h_{te}/c_m=0.1$ arose from a combination of several aerodynamic factors. With a reduced ground effect compared to prior configurations, alterations in lift distribution and vortex shedding patterns necessitated heightened roll stability due to reduced ground influence, reinstating the anhedral and dihedral.

The average parametric standard deviation at each of the four height-to-chord ratios is given in Table 3, and the average deviation of each of the 16 wing design parameters in Table 4. The standard deviations of the span and chord dimensions in Table 3 appear to be acceptable across the investigated height ratios. In contrast to the span and chord dimensions, the deviations in twist and sweep were larger. The deviation percentages in Table 4 for twist and sweep indicated substantial discrepancies, particularly for the twist angle. The discrepancies suggested that the said parameters might require further convergence for increased reliability in the design. The anhedral/dihedral angle standard deviations tabulated in Table 3 exhibited variations that differed across the height ratios. It is

worth noting that these variations were relatively consistent across the height ratios, which indicated a consistent pattern in design evolution. The percentages in Table 4 indicated notable deviations in anhedral/dihedral angles that warrant closer attention for convergence. While the deviation values for span and chord seemed reasonably consistent and within acceptable limits, the significant percentage deviations for parameters like twist, sweep, and anhedral/dihedral angles indicated potential convergence issues. These parameters appear to be more sensitive to the GA optimization process and might benefit from an additional number of generations to ensure more accurate results.

Table 3. Wing design average parameter standard deviation

	h_w/c_m			
	0.1	0.4	0.8	1.2
Span (m)	0.330	0.078	0.251	0.102
Chord (m)	0.169	0.088	0.074	0.085
Twist (deg.)	2.20	1.56	0.68	0.77
Sweep (deg.)	2.32	1.74	1.40	4.61
Anhedral/ Dihedral (deg.)	3.62	2.23	3.64	3.57

Table 4. Average deviation (%) indicating the non-converged wing design parameters

	Section	Average deviation (%)
Span (m)	2	2.0
	3	1.4
	4	0.6
Chord (m)	1	1.6
	2	1.8
	3	1.5
Twist (deg.)	4	4.8
	2	379.3
	3	166.6
Sweep (deg.)	4	76.8
	2	18.0
	3	39.6
Anhedral/Dihedral	4	22.6
	2	176.6
	3	49.0
	4	42.7

Comparing the best design of each of the four height-to-chord ratios as deemed by the fitness function given by eq. (1) with the datum case, yielded the results shown in Table 5.

The resultant L/D ratios obtained, were 16.3%, 14.1%, 39.0%, and 41.9% greater than the datum

case for $h_w/c_m=0.1, 0.4, 0.8, 1.2$, respectively. Hence, it followed that the wing loading criteria were slightly worse off than that of the base case; therefore, some adjustment may be needed to the fitness equation to rebalance the priority of the algorithm towards the wing loading criteria should it be deemed necessary.

Table 5. Resulting bioinspired variation having the best fitness value

h_w/c_m	Best Variation	Orlyonok Fitness value	Best Fitness Value
0.1	iii	88.52	+5.1%
0.4	iii	75.73	+74.8%
0.8	i	61.95	+7.6%
1.2	ii	50.16	+3.7%

5 Aircraft Flight Stability Effects

Having applied the genetic algorithm optimization and having resulted in a number of bioinspired wing designs potentially offering better L/D ratios to the original case study wing, the follow-on conceptual design step was to verify the aircraft compliance in terms of static and dynamic stability. AVL software is capable of generating linear static and dynamic stability margins and results about any flight equilibrium position, which for the present study the trimmed cruise case was assumed.

The case study aircraft had to be re-designed with versions of the bioinspired wings, with the respective AVL models depicted if Figure 10. For the sake of simplicity, the study aimed to inflict the minimum possible level of intervention upon the original aircraft design, in essence, to retain the existing aircraft fuselage and empennage. In the case of the project would be decided to be further matured, follow-up on studies would have needed to resize and relocate various features of the tailplane and fin structures. The bioinspired wings had to be located properly to replace the original Orlyonok A-90 case study wing. The optimized wings resulted in a certain anhedral angle for most designs, with the wing tips pointing towards the ground. It was suggested for the bioinspired wing placement to take place on the upper part of the fuselage, contrary to the case study aircraft which was a low wing placement aircraft design. The supposed wing mass that was altered due to higher aspect ratios, led to the proper positioning of the heavier wings at a longitudinal location that would retain the same aircraft center of gravity.

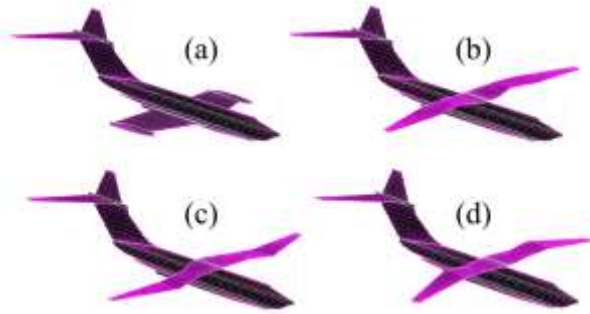


Fig. 10: AVL models for aircraft static and dynamic stability studies: (a) original A-90; (b), (c) & (d) modified wing A-90 versions

A conceptual design and a relatively simplistic approach to verifying the aircraft static stability is summarized in eq.(2) and (3), where the aero-derivatives of pitching (C_m) and yawing (C_n) moments concerning the pitching (α_{wb}) and yawing (β) angles are shown. The first equation, eq.(2), depicts the requirements for longitudinal static stability about the symmetry plane of the aircraft, while eq. (3) dictates the requirements for directional stability. Although a six-degree-of-freedom rigid aircraft of such designs can exhibit a certain level of coupling between rolling and yawing motion, only the directional stability aero-derivative was checked, as an initial design step.

$$\left(\frac{\partial C_m}{\partial \alpha_{wb}}\right) = C_{m\alpha} = \begin{cases} < 0 \rightarrow \text{Stable} \\ 0 \rightarrow \text{Neutral} \\ > 0 \rightarrow \text{Unstable} \end{cases} \quad (2)$$

$$\left(\frac{\partial C_n}{\partial \beta}\right) = C_{n\beta} = \begin{cases} < 0 \rightarrow \text{Unstable} \\ 0 \rightarrow \text{Neutral} \\ > 0 \rightarrow \text{Stable} \end{cases} \quad (3)$$

Evaluation of the aero-derivatives of eq. (2) and eq. (3) via AVL, showed that the bioinspired versions comply with the requirements of natural static stability, meaning that the modified aircraft can remain stable to perturbations about the trimmed cruise flight state, without the usage of electronic means of stability-enhancing. Dynamic stability was checked by plotting the root locus of the dynamic phugoid, short period, and Dutch roll modes. The location of the roots was captured on the positive complex plane for various heights from the ground and depicted in Figure 11, Figure 12 and Figure 13 for the original and unmodified A-90 aircraft; Figure 14, Figure 15 and 16 depict the root loci for representative modified A-90 aircraft with

bioinspired wings. From the above-mentioned figures, it was evidenced that the dynamic modes were stable, having roots with negative real part and similar damping levels for their decaying oscillatory motion.

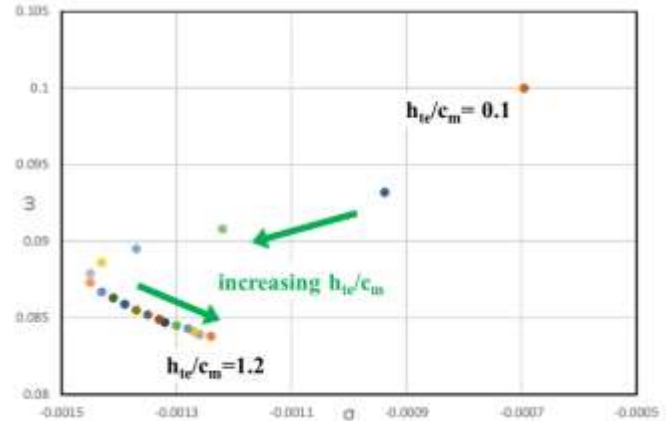


Fig. 11: Root locus for the phugoid mode of the original A-90 version

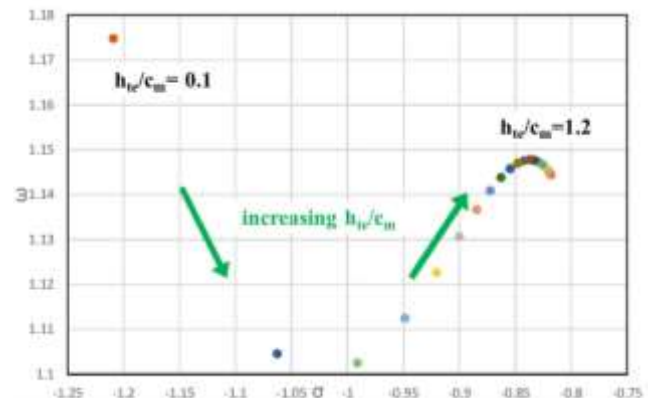


Fig. 12: Root locus for the short-period mode of the original A-90 version

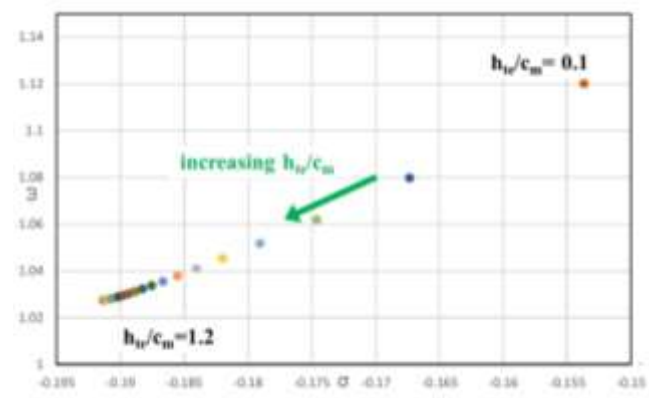


Fig. 13: Root locus for the Dutch roll mode of the original A-90 version

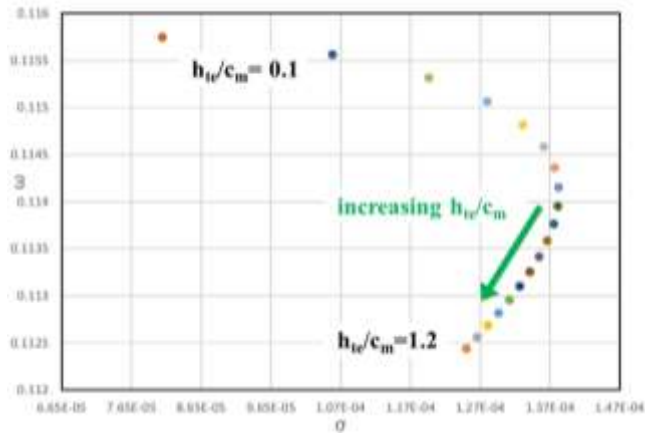


Fig. 14: Representative root locus plot of the phugoid mode for the bioinspired wing A-90

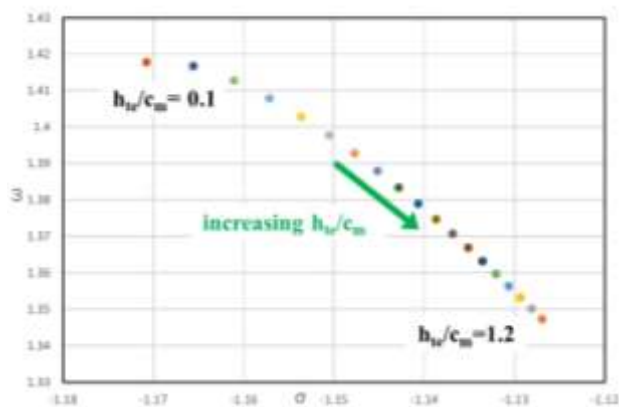


Fig. 15: Representative root locus plot of the short period mode for the bioinspired wing A-90

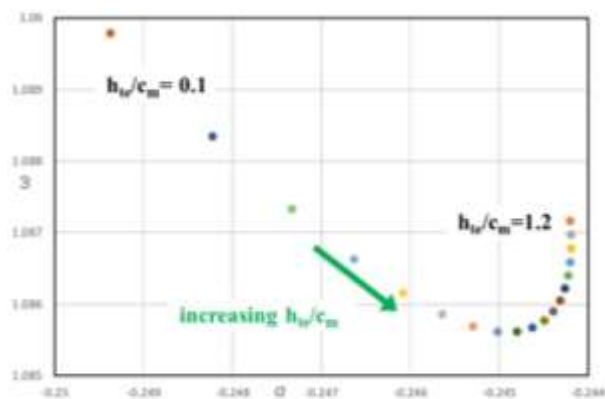


Fig. 16: Representative root locus plot of the Dutch roll mode for the bioinspired wing A-90

6 Conclusions

The Vortex Lattice CFD method was successfully applied in the present conceptual aircraft design optimization study, through the AVL software platform. Due to the rapid model generation and results evaluation software attributes, as well as the easiness in the coupling and internal communication

with Python, the study generated a genetic algorithm optimization loop that utilized the VLM input-output for results evaluation and subsequent modeling rebuilding based on the results, in a time efficient manner. The study resulted in conceptually reconstructing and successfully substituting the original wing of the A-90 Orlyonok WIG-craft, with bioinspired wing versions of enhanced L/D ratio.

As a second step, the study made use of the VLM method to draw preliminary conclusions and justifications for the static and dynamic stability of the resulting early conceptual design-level bioinspired wing modified aircraft.

The methodology presented herein along with the study results, provided an incremental step towards advancing Ground-Effect aircraft conceptual designs using VLM computational fluid dynamics.

References:

- [1] Yun L, Bliault A, Doo J, *WIG Craft and Ekranoplan: Ground Effect Craft Technology*, Springer US, 2010, DOI: 10.1007/978-1-4419-0042-5
- [2] Park K, Lee J, Influence of endplate on aerodynamic characteristics of low-aspect-ratio wing in ground effect, *Journal of Mechanical Science and Technology*, 22(12), 2578–2589, 2008, DOI: 10.1007/s12206-008-0805-y
- [3] Rozhdestvensky K, Pappas P, Karaminas E, Stubbs A, Pohl T, Hudson M, Stinton D, Thomasson P, *Ekranoplans: The GEMs of Fast Water Transport. Discussion, Transactions of the Institute of Marine Engineers*, 109(1), 47–74, 1997.
- [4] Halloran M, O'meara S, *Wing in Ground Effect Craft Review*. Melbourne Victoria, 1999.
- [5] Shirsath R A, Mukherjee R, Experimental and computational investigations of aerodynamic characteristics of a finite rectangular wing-inground effect, *Proceedings of the Institution of Mechanical Engineers, Part G Journal of Aerospace Engineering*, SAGE Publications Ltd, 2022, DOI: 10.1177/09544100221114700
- [6] Prandtl L, *Induced Drag of Multiplanes, NACA-TN-182*, 1965.
- [7] Boschetti P J, Quijada G M, Cárdenas E M, Dynamic ground effect on the aerodynamic coefficients of a wing using a panel method, *AIAA Atmospheric Flight Mechanics Conference. American Institute of Aeronautics*

- and Astronautics Inc.*, Washington, D.C., USA, 2016, DOI: 10.2514/6.2016-3104.
- [8] Suh Y B, Ostowari C O, Drag Reduction Factor Due to Ground Effect, *Journal of Aircraft*, 25(11): 1071–1072, 1988.
- [9] Laitone E V, Comment on Drag reduction factor due to ground effect, *Journal of Aircraft*, 27(1): 96–96, 1990.
- [10] Phillips W F, Hunsaker D F, Lifting-line predictions for induced drag and lift in ground effect, *31st AIAA Applied Aerodynamics Conference. American Institute of Aeronautics and Astronautics*, San Diego California, USA, 2013, DOI: 10.2514/6.2013- 2917.
- [11] Макаев P, Flying over the waves (Ekranoplan ‘Eaglet’), 1992.
- [12] Cervenka M, Zelinka I, Application of Evolutionary Algorithm on Aerodynamic Wing Optimisation, *2nd European Computing Conference*, Malta, p.344-348, 2008.
- [13] Drela M., Youngren H., AVL, [Online]. <https://web.mit.edu/drela/Public/web/avl/> (Accessed Date: April 26, 2024).
- [14] Zammit K, Smith H, Lobo N S, Giannopoulos I K, Vortex Lattice CFD Application and Modeling Validation for Ground Effect Aircraft, *WSEAS Transactions on Fluid Mechanics*, Vol. 19, 2024, pp.49-58, <https://doi.org/10.37394/232013.2024.19.5>.
- [15] Gehrke A, Guyon-Crozier G, Mulleners, K, Genetic Algorithm Based Optimization of Wing Rotation in Hover, *Fluids*, 3(3), 59, 2018, DOI: 10.3390/fluids3030059.
- [16] Cayiroglu I, Kilic R, Wing Aerodynamic Optimization by Using Genetic Algorithm and Ansys, *Acta Physica Polonica A*, 132(3–II), pp.981-985. 2017, DOI: 10.12693/APhysPolA.132.981.
- [17] Holst T L, Pulliam T H, Transonic Wing Shape Optimization Using a Genetic Algorithm, in *Sobieczky, H. (ed.) IUTAM Symposium Transsonicum IV. Fluid Mechanics and its Applications*. Springer, 245–252, 2003, DOI: 10.1007/978-94-010-0017-8_38.
- [18] Lai K K, Mishra S K, Sharma R, Sharma M, Ram B, A Modified q-BFGS Algorithm for Unconstrained Optimization, *Mathematics*, 11(6), 1420, 2023, DOI: 10.3390/math11061420.
- [19] Tutorialspoint Crossover, Genetic Algorithms Tutorial, [Online]. https://www.tutorialspoint.com/genetic_algorithms/genetic_algorithms_crossover.htm (Accessed Date: April 26, 2024).
- [20] Tutorialspoint Parent Selection, Genetic Algorithms Tutorial, [Online]. https://www.tutorialspoint.com/genetic_algorithms/genetic_algorithms_parent_selection.htm (Accessed Date: April 26, 2024).

Contribution of Individual Authors to the Creation of a Scientific Article (Ghostwriting Policy)

- Karl Zammit: methodology, investigation, formal analysis, software, validation
- Howard Smith: conceptualization, supervision, project administration
- Noel Sierra Lobo: methodology, investigation, formal analysis, software, validation
- Ioannis K. Giannopoulos: validation, visualization, writing

Sources of Funding for Research Presented in a Scientific Article or Scientific Article Itself

No funding was received for conducting this study.

Conflict of Interest

The authors have no conflicts of interest to declare.

Creative Commons Attribution License 4.0 (Attribution 4.0 International, CC BY 4.0)

This article is published under the terms of the Creative Commons Attribution License 4.0

https://creativecommons.org/licenses/by/4.0/deed.en_US